Polymer Chemistry

PAPER

View Article Online
View Journal | View Issue

Published on 13 March 2017. Downloaded by Synchrotron Radiation Library on 12/12/2017 06:44:24.

Check for updates

Cite this: *Polym. Chem.*, 2017, **8**, 2334

Synthesis and side-chain isomeric effect of 4,9-/5,10-dialkylated-β-angular-shaped naphthodithiophenes-based donor–acceptor copolymers for polymer solar cells and field-effect transistors†

De-Yang Chiou,[a] Fong-Yi Cao,[a] Jhih-Yang Hsu,[a] Che-En Tsai,[a] Yu-Ying Lai,[b] U-Ser Jeng,[c,d] Jianquan Zhang,[e] He Yan,[e] Chun-Jen Su[c] and Yen-Ju Cheng *[a]

Received 2nd February 2017,
Accepted 13th March 2017

DOI: 10.1039/c7py00194k

rsc.li/polymers

A systematic methodology is developed to construct the angular-shaped β-form naphthodithiophene (β-aNDT) core with regiospecific substitution of two alkyl groups at its 4,9- or 5,10-positions *via* the base-induced double 6π-cyclization of dithienyldieneyne precursors, leading to the two isomeric 4,9-β-aNDT and 5,10-β-aNDT monomers. It is found that a more curved geometry of the β-aNDT units intrinsically increases the solubility and thus the solution-processability of the resultant polymers. Therefore, β-aNDT units are ideal for polymerization with an acceptor-containing monomer without the need for any solubilizing aliphatic side chains, which are considered the insulating portion that jeopardizes charge transport. Based on this consideration, the 4,9- and 5,10-dialkylated β-aNDT monomers are polymerized with the non-alkylated DTFBT acceptor to afford two **P4,9-βNDTDTFBT** and **P5,10-βNDTDTFBT** copolymers for head-to-head comparison of the 4,9-inner/5,10-outer isomeric alkylation effect. It is found that 4,9-β-aNDT adopts a twisted conjugated structure due to the intramolecular steric repulsion between the inner branched side chains and the β-hydrogens on the thiophene rings. The slightly twisted 4,9-β-aNDT moiety allows **P4,9-βNDTDTFBT** to have higher solubility upon polymerization and thus a higher molecular weight, which eventually induces a higher ordered packing structure in the thin film compared to **P5,10-βNDTDTFBT**. As a result, **P4,9-βNDTDTFBT** exhibits a higher OFET mobility of 0.18 $cm^2 V^{-1} s^{-1}$, and the **P4,9-βNDTDTFBT**:$PC_{71}BM$-based solar cell device also achieves a higher PCE of 7.23%, which is even better than the corresponding **P4,9-αNDTDTFBT**-based device.

Introduction

Conjugated donor–acceptor copolymers have been widely used in organic photovoltaics (OPVs) and organic field effect transistors (OFETs).[1–20] Considerable research has been directed to the development of new donor building blocks for the construction of donor–acceptor (D–A) copolymers.[21–30] The acenedithiophenes (AcDT) have been demonstrated as superior building blocks due to their rigid and coplanar architectures for efficient charge transport and selective C_2-functionalization of the terminal thiophenes for π-extension. Among the members in the AcDT family, the benzodithiophene (BDT)-based[7,29,31–35] and also the anthradithiophene(ADT)-based[36–45] D–A copolymers have successfully achieved high performances in OPV and OFET applications, respectively. Very recently, tetracyclic naphthodithiophenes (NDTs)[46–54] have also emerged as promising materials but with much less research exploration. "Zigzag" angular-shaped NDT (aNDT) units in the *anti*-orientation have particularly received appreciable attention, considering that the copolymer incorporated in the aNDT units packs into higher ordered structures to achieve higher OFET mobilities in comparison with polymers employing linear-fused NDT (lNDT) units.[52,53] The sulfur atoms can be attached on the α- or β-positions of the central naphthalene moiety in aNDTs, yielding two regioisomers denoted as α-aNDT and β-aNDT, respectively (Scheme 1). It is necessary to

[a]*Department of Applied Chemistry, National Chiao Tung University, 1001 University Road, Hsinchu, 30010 Taiwan. E-mail: yjcheng@mail.nctu.edu.tw*
[b]*Institute of Polymer Science and Engineering, National Taiwan University, Taipei, 10617 Taiwan*
[c]*National Synchrotron Radiation Research Center, 101 Hsin-Ann Road, Hsinchu Science Park, Hsinchu 30076, Taiwan*
[d]*Department of Chemical Engineering, National Tsing Hua University, Hsinchu 30013, Taiwan*
[e]*Department of Chemistry and Energy Institute, The Hong Kong University of Science and Technology, Clear Water Bay, Kowloon, Hong Kong, China*
†Electronic supplementary information (ESI) available. See DOI: 10.1039/c7py00194k

This journal is © The Royal Society of Chemistry 2017

Published on 13 March 2017. Downloaded by Synchrotron Radiation Library on 12/12/2017 06:44:24.

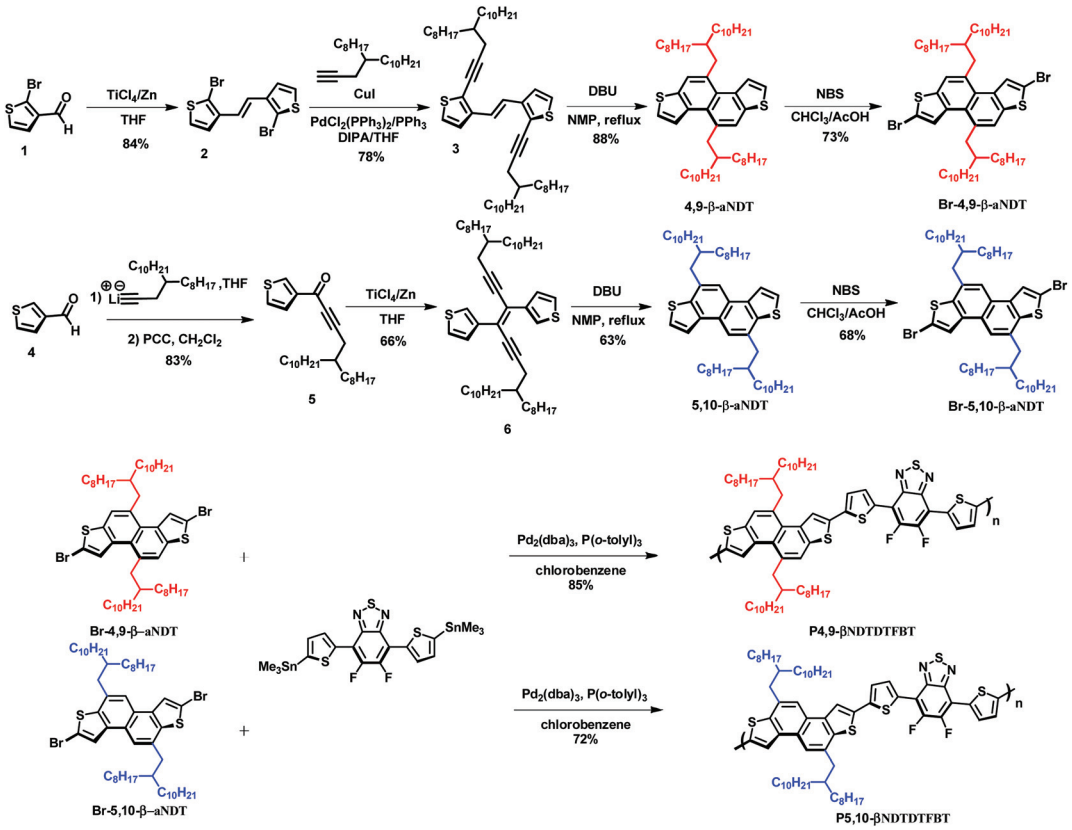

Scheme 1 Synthesis of the Br-4,9-β-aNDT and Br-5,10-β-aNDT monomers and their corresponding polymers.

introduce aliphatic side chains to bare aNDT moieties as solubilizing groups toward polymer synthesis. To this end, we develop a systematic strategy to implant two alkyl groups at the 4,9- or 5,10-positions of α-aNDT and β-aNDT units, leading to the formation of four isomeric 4,9- and 5,10-dialkylated α-aNDT structures as well as 4,9- and 5,10-dialkylated β-aNDTs. The two isomeric 4,9-α-aNDT and 4,9-β-aNDT monomers are copolymerized with dithienylnaphthobisthiadiazole (DTNT) monomer to form **PαNDTDTNT** and **PβNDTDTNT**, (Fig. 1) to systematically investigate the α- and β- main-chain isomeric effect.[51]

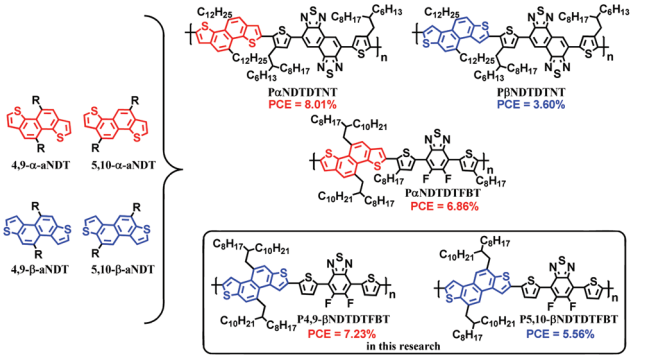

Fig. 1 Chemical structures of the four isomeric dialkylated α-aNDT and β-aNDT and the aNDT-based copolymers in the literature and in this research.

We found that the geometry of the α-aNDT moiety results in a more linear polymeric backbone than the β-aNDT counterpart. The less curved conjugated main chain facilitates stronger intermolecular π–π interactions compared to the **PβNDTDTNT** counterpart. As a result, the **PαNDTDTNT**-based device delivered a higher OFET mobility and superior solar-cell efficiency of 8.01% that outperformed the **PβNDTDTNT**-based device with a moderate power conversion efficiency (PCE) of 3.6%.[51] On the other hand, the 4,9-α-aNDT monomer was also copolymerized with the dioctyldithienyldifluorobenzothiadiazole (DTFBT) monomer to form the corresponding **PαNDTDTFBT**, which also exhibited a decent efficiency of 6.86% (Fig. 1).[50]

It is documented that the incorporation of bulky aliphatic side chains close to the acceptor subunit might sterically hinder the photo-induced electron transfer from the D–A copolymer to fullerene materials.[57,58] In view of the fact that the geometry of β-aNDT gives rise to a more curved conjugated main chain and thus less closely packed structure, the β-aNDT-based copolymers possess much better solubility compared to the corresponding α-aNDT-based copolymers. We envision that the molecular properties and device performance of β-aNDT-based D–A copolymers could be further modulated and improved by cutting off the insulating aliphatic side chains installed near the acceptor units without largely affecting the polymer solubility. Furthermore, the 5,10-dialkyl β-aNDT unit with two alkyl groups at the outer 5,10-positions

Published on 13 March 2017. Downloaded by Synchrotron Radiation Library on 12/12/2017 06:44:24.

has never been incorporated into D–A copolymers. The position of the aliphatic side chains might dramatically influence the solubility, crystallization, molecular packing and thus charge transportation of the polymers, resulting in variations in device performance.[57–64] It is therefore of great interest to head-to-head compare the inner (4,9-dialkyl) and outer (5,10-dialkyl) side-chain isomeric effect of the β-aNDT motifs on the resulting D–A copolymer properties. In this research, two 4,9-di(2-octyldodecyl) β-aNDT and 5,10-di(2-octyldodecyl) β-aNDT monomers were synthesized and polymerized with a dithienyl-5,6-difluoro-2,1,3-benzothiadiazole (DTFBT) monomer, which does not contain any aliphatic side-chain groups on the thienyl units next to the central FBT acceptor unit, affording two new copolymers **P4,9-βNDTDTFBT** and **P5,10-βNDTDTFBT** with adequate solution-processability (Fig. 1). The molecular properties, device performance and isomeric effect[51–53,55,56] of the new polymers are discussed.

Results and discussion

Synthesis

The synthetic routes for the **Br-4,9-β-aNDT** and **Br-5,10-β-aNDT** monomers are illustrated in Scheme 1. Nucleophilic addition of (3-octyltridecylidyne)lithium to thiophene-3-carboaldehyde (**4**), followed by pyridinium chlorochromate (PCC) oxidation yielded compound **5**. Dimerization of 2-bromothiophene-3-carboaldehyde **1** and **5** by McMurry condensation formed the olefinic products **2** and **6**, respectively, with the *E*-form as the major olefinic configuration. The alkynylation of **2** with 9-(prop-2-yn-1-yl)nonadecane by the Sonogashira coupling reaction afforded the dialkynylated compound **3**. The desired isomeric **4,9-β-aNDT** as well as **5,10-β-aNDT** were successfully obtained by the 1,8-diazabicycloundec-7-ene (DBU)-induced intramolecular tandem 6π-cyclization of **3** and **6**. Double bromination of **4,9-β-aNDT** and **5,10-β-aNDT** was selectively carried out at the 2,7-positions using *N*-bromosuccinimide (NBS) to yield **Br-4,9-β-aNDT** and **Br-5,10-β-aNDT**. The two brominated monomers were copolymerized with the Sn-DTFBT monomer by Stille coupling to afford **P4,9-βNDTDTFBT** and **P5,10-βNDTDTFBT**, respectively. The molecular weight (M_n) was determined to be 24.5 kDa with a polydispersity index (PDI) of 1.9 for **P4,9-βNDTDTFBT** and 16.1 kDa with a PDI of 1.6 for **P5,10-βNDTDTFBT** by gel permeation chromatography (GPC) measurement. Even though the two polymers have only two aliphatic side chains on the β-aNDT units, **P4,9-βNDTDTFBT** and **P5,10-βNDTDTFBT** can be completely dissolved in hot dichlorobenzene solution (5 mg mL^{-1}) at 80 °C and 100 °C, respectively, which indicates that **P4,9-βNDTDTFBT** has better solubility than **P5,10-βNDTDTFBT**.

Thermal properties

P4,9-βNDTDTFBT and **P5,10-βNDTDTFBT** did not show thermal transition peaks in the differential scanning calorimetry (DSC) measurements; from the thermogravimetric analysis (TGA), the polymers exhibit high decomposition temperatures (T_d) of 468 and 450 °C, respectively (Fig. 2).

Electrochemical properties

Electrochemical properties of the polymers were determined by cyclic voltammetry (CV) (Fig. 3) and their characteristics are shown in Table 1. The highest occupied molecular orbital (HOMO) energy levels of the small molecules **4,9-β-aNDT** and **5,10-β-aNDT** were estimated to be −5.72 and −5.66 eV, respectively. The LUMO energy levels calculated by HOMO + optical bandgap (E_g^{opt}) were determined to be −2.10 and −2.14 eV for **4,9-β-aNDT** and **5,10-β-aNDT**, respectively. The two polymers exhibited stable and reversible electrochemical characteristics during the oxidative and reductive scans. The HOMO levels of **P4,9-βNDTDTFBT** and **P5,10-βNDTDTFBT** are approximately

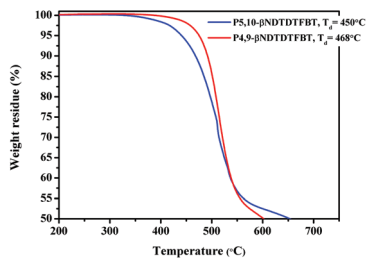

Fig. 2 Thermogravimetric analysis of **P4,9-βNDTDTFBT** and **P5,10-βNDTDTFBT** at a ramping rate of 10 °C min^{-1}.

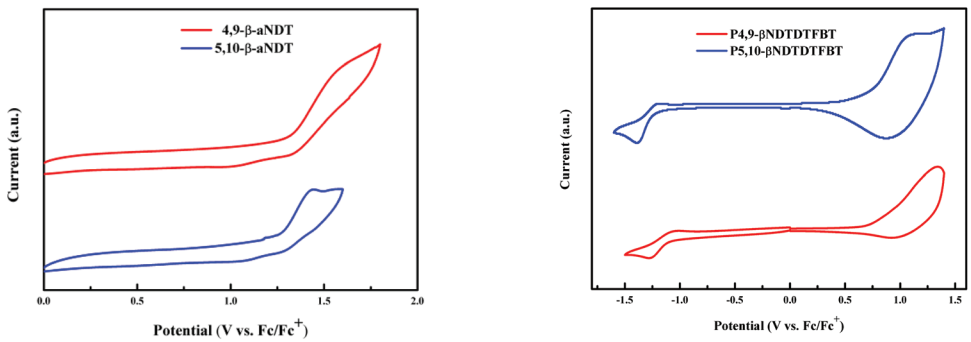

Fig. 3 CV curves of **4,9-β-aNDT**, **10-β-aNDT**, **P4,9-βNDTDTFBT** and **P5,10-βNDTDTFBT** at a scanning rate of 50 mV s^{-1}.

 This journal is © The Royal Society of Chemistry 2017

Published on 13 March 2017. Downloaded by Synchrotron Radiation Library on 12/12/2017 06:44:24.

Table 1 Electrochemical and thermal properties of 4,9-β-aNDT, 5,10-β-aNDT, P4,9-βNDTDTFBT and P5,10-βNDTDTFBT

Copolymer	T_d (°C)	HOMO (eV)	LUMO[c] (eV)	E_g^{ele} (eV)	E_g^{opt} (eV)	M_n (kDa)	M_w (kDa)	PDI
4,9-β-aNDT[a]	—	−5.72	−2.10	—	3.62	—	—	—
5,10-β-aNDT[a]	—	−5.66	−2.14	—	3.52	—	—	—
P4,9-βNDTDTFBT[b]	468	−5.55	−3.70	1.85	1.76	24.5	47.1	1.9
P5,10-βNDTDTFBT[b]	450	−5.49	−3.61	1.88	1.74	16.1	25.8	1.6

[a] Measured in CH_2Cl_2. [b] Measured in acetonitrile. [c] LUMO levels were calculated by HOMO + E_g^{opt}.

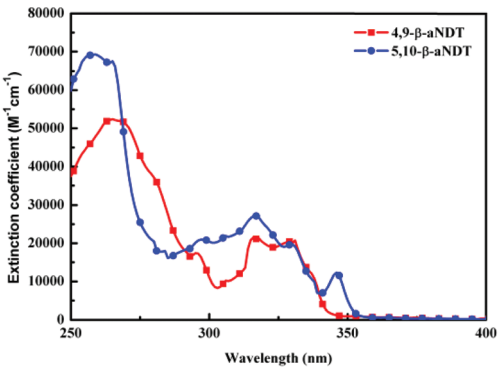

Fig. 4 UV-Vis absorption spectra of **4,9-β-aNDT** and **5,10-β-aNDT** in *o*-DCB with a concentration of 10 μM.

located at −5.55 eV and −5.49 eV, respectively. Moreover, the lowest unoccupied molecular orbital (LUMO) levels are estimated to be −3.70 eV for **P4,9-βNDTDTFBT** and −3.61 eV for **P5,10-βNDTDTFBT**, which are higher than the LUMO level of $PC_{71}BM$ (−3.8 eV) for favorable electron transfer. The estimated electronic band gap of **P4,9-βNDTDTFBT** (1.85 eV) is slightly lower than that of **P5,10-βNDTDTFBT** (1.88 eV).

Optical properties

The UV-Vis absorbance spectra of **4,9-β-aNDT** and **5,10-β-aNDT** measured in orthodichlorobenzene (*o*-DCB) are illustrated in Fig. 4. Although **4,9-β-aNDT** and **5,10-β-aNDT** have identical conjugated backbones, the difference in the side-chain substitution positions makes the profile of the absorption spectra different. **5,10-β-aNDT** with the outer alkylation essentially

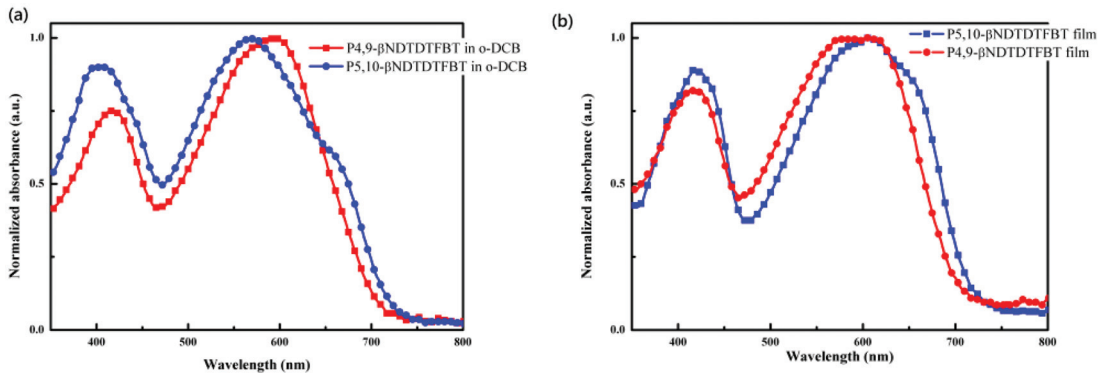

Fig. 5 Normalized UV-Vis absorption spectra of the (a) solution state and (b) film state of **P4,9-βNDTDTFBT** and **P5,10-βNDTDTFBT**.

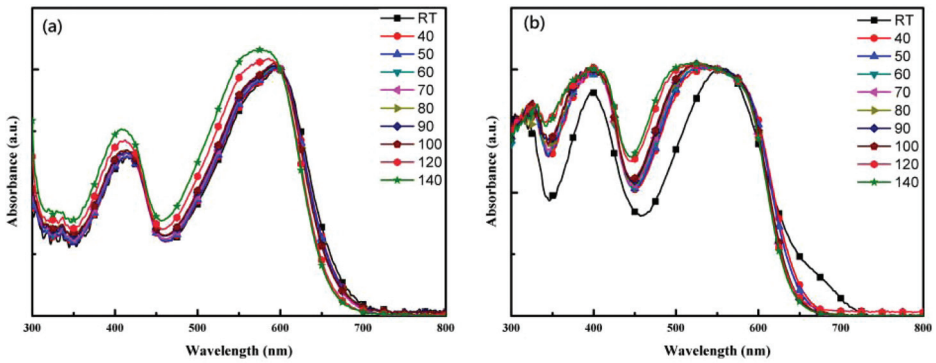

Fig. 6 Solution state temperature dependent UV-Vis absorption spectra of (a) **P4,9-βNDTDTFBT** and (b) **P5,10-βNDTDTFBT** in *o*-DCB.

Published on 13 March 2017. Downloaded by Synchrotron Radiation Library on 12/12/2017 06:44:24.

shows higher extinction coefficient red-shifted bands at around 300 to 350 nm and thus a smaller optical bandgap compared to **4,9-β-aNDT** with inner alkylation. The normalized absorption spectra of the two polymers show two distinct bands (Fig. 5). Similar to the smaller molecules, **P5,10-βNDTDTFBT** exhibits a slightly smaller optical band gap of 1.74 eV than **P4,9-βNDTDTFBT** with 1.76 eV estimated from the onset of the thin film absorption spectra. The temperature-dependent absorption spectra were measured at room temperature (rt), 40, 50, 60, 70, 80, 90, 100, 120, and 140 °C (Fig. 6). The absorbance of the two polymers gradually blue-shifted as the temperature increased, suggesting that the polymeric interchain interactions occurring at room temperature are weakened at high temperatures as a result of increased thermal motion around the polymer main chains.[65] From rt to 140 °C, the λ_{max} of **P4,9-βNDTDTFBT** and **P5,10-βNDTDTFBT** is blue-shifted by 12 and 43 nm, respectively, which implies that **P5,10-βNDTDTFBT** might have stronger intermolecular interactions in solution (Table 2).

Table 2 Optical properties of 4,9-β-aNDT, 5,10-β-aNDT, P4,9-βNDTDTFBT and P5,10-βNDTDTFBT

Compound	λ_{max} (nm)		λ_{onset} (nm)	E_g^{opt} (eV)
	o-DCB	Film		
4,9-β-aNDT	265	—	342[a]	3.63
5,10-β-aNDT	258	—	352[a]	3.52
P4,9-βNDTDTFBT	416, 594	417, 605	705	1.76
P5,10-βNDTDTFBT	406, 567	413, 604	714	1.74

[a] Obtained from solution state UV-Vis absorption spectrum.

Theoretical calculations

In order to gain insight into the inner/outer side-chain isomeric effects on the **β-aNDT** main-chain structure, geometry optimization of the **4,9-β-aNDT** and **5,10-β-aNDT** structures was performed at the B3LYP/6-31G(d) level of theory. As shown in Fig. 7(a), unlike **5,10-β-aNDT**, which exhibits a coplanar conjugated structure, **4,9-β-aNDT** shows a twisted structure with a dihedral angle of 12.3° between the two benzothiophene subunits. This distorted structure of **4,9-β-aNDT** clearly is a result

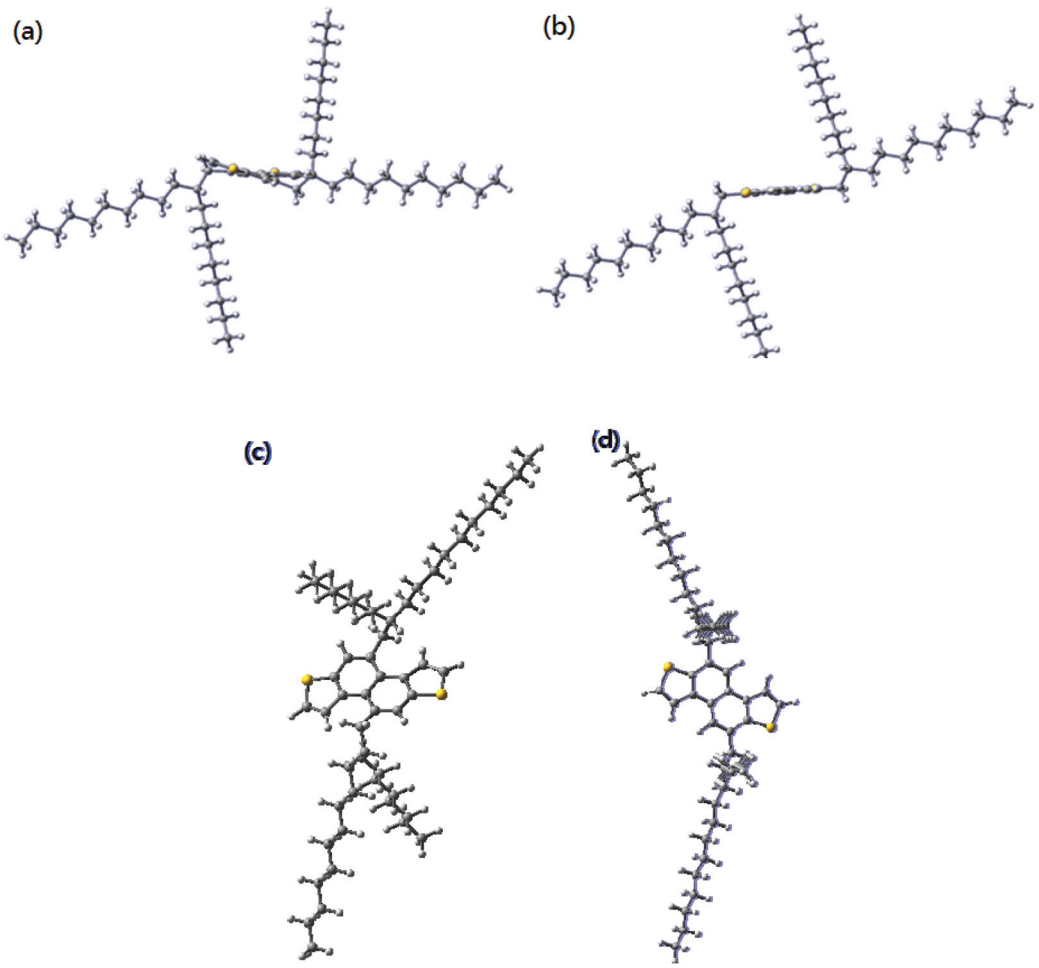

Fig. 7 Side (a and b)/top (c and d) view of the optimized geometry of **4,9-β-aNDT** and **5,10-β-aNDT**, respectively, calculated at the level of B3LYP/6-31G(d).

 This journal is © The Royal Society of Chemistry 2017

Published on 13 March 2017. Downloaded by Synchrotron Radiation Library on 12/12/2017 06:44:24.

of the steric repulsion between the hydrogens on the second carbon of the branched alkyl chains and the β-hydrogens on the thiophene units. Compared to its **5,10-β-aNDT** counterpart, the distorted structure of the **4,9-β-aNDT** units in the polymer might slightly shorten the effective conjugation length and weaken the intermolecular interactions. This structural disparity could rationally explain the phenomena discussed previously: (1) **5,10-β-aNDT** and **P5,10-βNDTDTFBT** show slightly smaller optical bandgaps and stronger intermolecular interactions than the corresponding **4,9-β-aNDT** and **P4,9-βNDTDTFBT**; (2) **P4,9-βNDTDTFBT** intrinsically has much higher solubility than **P5,10-βNDTDTFBT** due to its less tendency for aggregation, leading to a much higher molecular weight. (3) **4,9-β-aNDT** and **P4,9-βNDTDTFBT** have slightly lower-lying HOMO energy levels.

Transistor characterization

OFET devices using the bottom-gate/bottom-contact configuration with evaporated gold source/drain electrodes were fabricated to evaluate the mobilities of the polymers. The surfaces of SiO_2 as the gate dielectric were modified with octadecyltrichlorosilane (ODTS) to form a self-assembled monolayer (SAM). The polymer films prepared by spin-coating from chlorobenzene (CB) solutions were subsequently annealed at 200 °C. All the output and transfer plots of the devices show typical p-type OFET characteristics (Fig. 8). The hole mobilities listed in Table 3 with on/off ratios were calculated from the transfer characteristics of the devices in the saturation regime. The **P4,9-βNDTDTFBT** and **P5,10-βNDTDTFBT** devices without thermal annealing exhibit hole mobilities of 0.025 $cm^2\ V^{-1}\ S^{-1}$ and 6.4×10^{-4} $cm^2\ V^{-1}\ S^{-1}$, respectively. After thermal annealing at 200 °C, the mobilities dramatically improve to 0.18 $cm^2\ V^{-1}\ S^{-1}$ for **P4,9-βNDTDTFBT** and 0.058 $cm^2\ V^{-1}\ S^{-1}$ for **P5,10-βNDTDTFBT**. The higher mobility of **P4,9-βNDTDTFBT** might be ascribed to its much higher molecular weight.

Table 3 P-type OFET characteristics of the polymers

Copolymer	Annealing (°C)	V_{th} (V)	$I_{on/off}$	Mobility ($cm^2\ V^{-1}\ s^{-1}$)
P4,9-βNDTDTFBT	—	−19.5	6.26×10^7	0.025
P4,9-βNDTDTFBT	200	−23.9	1.30×10^7	0.18
P5,10-βNDTDTFBT	—	−21.6	3.43×10^4	6.4×10^{-4}
P5,10-βNDTDTFBT	200	−28.1	5.83×10^7	0.058

Photovoltaic characteristics

Bulk heterojunction devices with an inverted architecture ITO/ZnO/polymer:$PC_{71}BM$/MoO_3/Ag were thus fabricated. The current density–voltage characteristics and the external quantum efficiency (EQE) spectra of the devices under simulated 100 mW cm^{-2} at AM1.5G illumination are shown in Fig. 9 and the device parameters are shown in Table 4. The device using the **P4,9-βNDTDTFBT**:$PC_{71}BM$ (1 : 1 wt%) blend with 5 vol% diphenyl ether (DPE) as an additive delivered a PCE of 7.01% with a V_{oc} of 0.88 V, moderate J_{sc} of −11.57 mA cm^{-2}, and a fill factor (FF) of 68.88%. To make a consistent comparison, the **P5,10-βNDTDTFBT**:$PC_{71}BM$ based device using identical fabrication conditions (1 : 1 wt% with 5 vol% DPE) showed a PCE of 5.08%, with a J_{sc} of −11.26 mA cm^{-2}, V_{oc} of 0.72 V, and FF of 62.63%. The PCE of both **P4,9-βNDTDTFBT**- and **P5,10-βNDTDTFBT**-based devices can be further improved to 7.23% and 5.56%, respectively (Table 4).

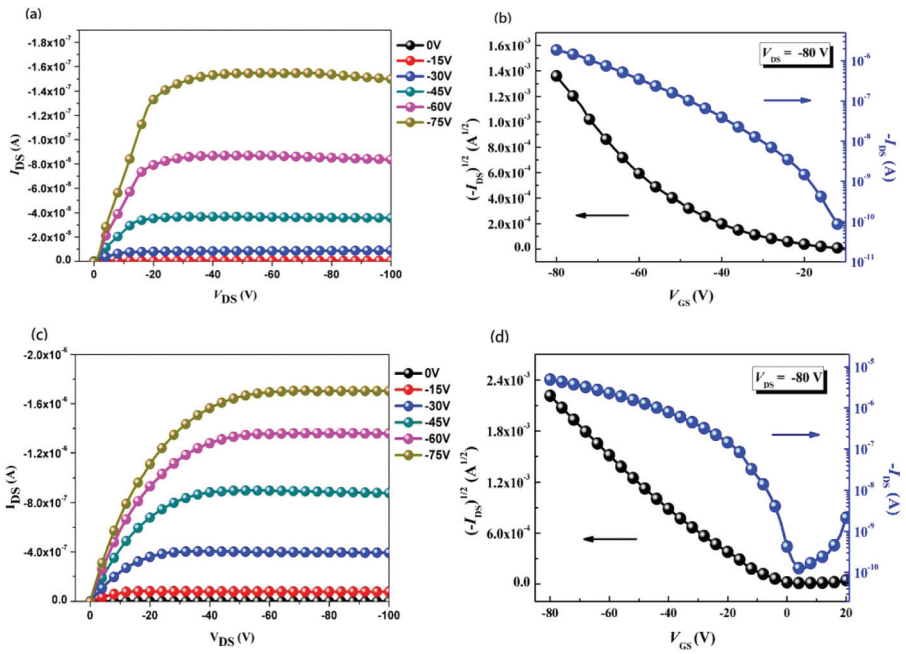

Fig. 8 Typical output curves (a, c) and transfer plots (b, d) of the OFET devices based on **P4,9-βNDTDTFBT** and **P5,10-βNDTDTFBT**, respectively.

Published on 13 March 2017. Downloaded by Synchrotron Radiation Library on 12/12/2017 06:44:24.

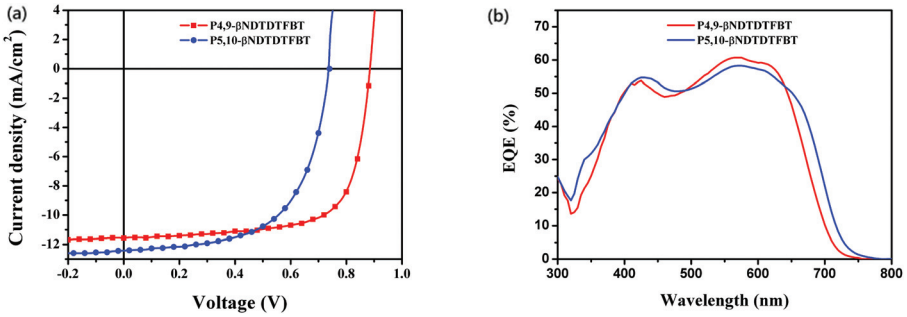

Fig. 9 (a) *J*–*V* curves and (b) EQE plots of the **P4,9-βNDTDTFBT**-based and **P5,10-βNDTDTFBT**-based devices.

Table 4 Photovoltaic parameters of the ITO/ZnO/polymer:$PC_{71}BM$/MoO_3/Ag devices

Copolymer	Polymer: $PC_{71}BM$[a] (wt% ratio)	Spin rate (rpm)	V_{oc} (V)	J_{sc} (mA cm^{-1})	PCE (%)	FF (%)
P4,9-βNDTDTFBT	1 : 1	800	0.88	−11.57	7.01	68.88
P4,9-βNDTDTFBT	1 : 2[b]	1200	0.88	−11.56	7.23	71.03
P5,10-βNDTDTFBT	1 : 1	800	0.72	−11.26	5.08	62.63
P5,10-βNDTDTFBT	1 : 1	1200	0.74	−12.42	5.56	60.48

[a] Polymer concentration of 15 mg mL^{-1} with 5 vol% diphenyl ether (DPE) as an additive and *o*-DCB as the solvent. [b] Polymer concentration of 13 mg mL^{-1}.

The higher molecular weight of **P4,9-βNDTDTFBT** in comparison with **P5,10-βNDTDTFBT** might be the major reason for its higher efficiency. It should be emphasized that by molecular engineering of the polymer structure, the **β-NDT**-based **P4,9-βNDTDTFBT** can exhibit a better performance than the corresponding **α-NDT**-based **P4,9-αNDTDTFBT** copolymer (Fig. 1).[50]

X-ray diffraction measurements

2D grazing-incidence wide-angle X-ray diffraction (2D-GIWAXRD) was conducted to investigate the thin film morphologies of the neat polymers and polymer/$PC_{71}BM$ blends (Fig. 10). Compared to **P5,10-βNDTDTFBT**, **P4,9-βNDTDTFBT** exhibits stronger high-order lamellar stacking peaks in the

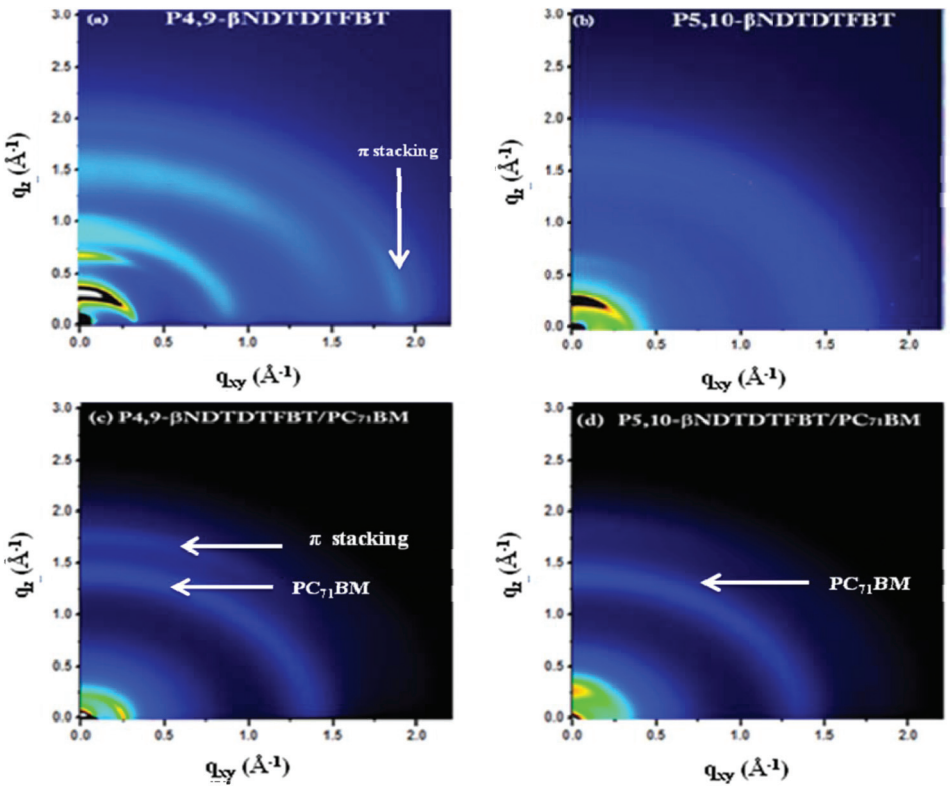

Fig. 10 2D-GIXRD patterns of the (a) **P4,9-βNDTDTFBT**; (b) **P5,10-βNDTDTFBT**; (c) **P4,9-βNDTDTFBT**:$PC_{71}BM$ and (d) **P5,10-βNDTDTFBT**:$PC_{71}BM$ blends.

 This journal is © The Royal Society of Chemistry 2017

Published on 13 March 2017. Downloaded by Synchrotron Radiation Library on 12/12/2017 06:44:24.

out-of-plane direction and a π-stacking peak at q_{xy} = 1.83 Å^{-1} in the in-plane direction corresponding to the π-stacking (edge-on) with a distance of *ca.* 3.43 Å (Fig. 10a and b), which is believed to facilitate the charge transport along the OFET transport channel. The higher ordering of **P4,9-βNDTDTFBT** relative to **P5,10-βNDTDTFBT** is likely to be associated with its better solubility, which allows more time for the polymer to pack during solvent evaporation from the film. Consequently, **P4,9-βNDTDTFBT** has a hole mobility of 0.18 cm^2 V^{-1} S^{-1}, which is 3-fold higher than that of **P5,10-βNDTDTFBT** with 0.058 cm^2 V^{-1} S^{-1}. Compared to **P5,10-βNDTDTFBT**:$PC_{71}BM$ (1 : 1 wt%), the **P4,9-βNDTDTFBT**:$PC_{71}BM$ thin film shows a more pronounced out-of-plane diffraction peak at q_z = 1.71 Å^{-1}, corresponding to the π-stacking with a distance of *ca.* 3.67 Å (Fig. 10c), suggesting that **P4,9-βNDTDTFBT** tends to adopt a face-on orientation in the blend, which is beneficial for vertical charge transport in the active layer. Interestingly, the π-stacking of **P4,9-βNDTDTFBT** changes from the edge-on to face-on orientation after the incorporation of $PC_{71}BM$, which is an indication of stronger association with $PC_{71}BM$, thereby resulting in the higher filling factor of the **P4,9-βNDTDTFBT**:$PC_{71}BM$-based device.

Conclusions

Compared to the α-aNDT unit, studies have shown that the molecular geometry of the β-aNDT building block, which leads to a more curved backbone of β-aNDT-based polymers, is not ideal for the formation of ordered structures in the solid state. Nevertheless, such a structural configuration also simultaneously imparts much better solubility to β-aNDT-based polymers. On the basis of this characteristic, we rationalize that the charge transport of β-aNDT-based polymers can be improved by reducing the content of insulating aliphatic groups near the acceptor units without encountering poor solution-processability. In addition, the inner or outer dialkylation of β-aNDT might play an important role in determining the molecular properties and organic electronic applications, which are worthy of investigation. To this end, we have successfully synthesized two regiospecific 4,9-di(2-octyldodecyl) β-aNDT and 5,10-di(2-octyldodecyl)-β-aNDT isomeric monomers, which were further copolymerized with a non-alkylated DTFBT monomer to afford the two polymers **P4,9-βNDTDTFBT** and **P5,10-βNDTDTFBT** with adequate solution-processability. Although the 4,9-β-aNDT and 5,10-β-aNDT molecules have identical conjugated backbones, theoretical calculation suggests that 4,9-β-aNDT actually forms a twisted structure due to the steric congestion between the inner alkyl groups and the β-hydrogens on the fused thiophene units, whereas the 5,10-β-aNDT molecule with outer alkylation still maintains a planar structure. The twisted 4,9-β-aNDT units in **P4,9-βNDTDTFBT** might reduce the intermolecular interactions. Therefore, **P4,9-βNDTDTFBT** possesses much higher solubility than **P5,10-βNDTDTFBT**, thus yielding a higher molecular weight during polymerization. Due to the higher ordered molecular packing in the solid state associated with its higher M_n, **P4,9-βNDTDTFBT** shows a higher OFET hole mobility of 0.18 cm^2 V^{-1} S^{-1} than **P5,10-βNDTDTFBT** with 0.058 cm^2 V^{-1} S^{-1}. Furthermore, the **P4,9-βNDTDTFBT**:$PC_{71}BM$-based device exhibits an efficiency of 7.23% which is also superior to the **P5,10-βNDTDTFBT**:$PC_{71}BM$-based device, thus indicating that inner/outer isomeric side-chain variation of β-NDT indeed can further modulate the microscopic properties and macroscopic performance of the polymers. Notably, by cutting off the aliphatic side chains in the polymer, the β-NDT-based **P4,9-βNDTDTFBT** can ultimately exhibit an even better performance than the corresponding α-NDT-based **PαNDTDTFBT** copolymer.[50] This research demonstrates that the dialkyl β-NDT units can function as promising building blocks for the fabrication of semiconductor polymers as long as proper molecular engineering can be smartly implemented. Further exploration of β-NDT-based copolymers is still ongoing in our laboratory.

Experimental

Materials

Unless otherwise stated, all reactions were carried out in a vacuum line under N_2 atmosphere. Commercially available chemicals were used as received and all solvents were distilled before use. 2-Bromothiophene-3-carbaldehyde (**1**) was synthesized as reported.[46]

Instrumentation

^{1}H and ^{13}C NMR spectra were measured using a Varian 400 MHz spectrometer and obtained in deuterated chloroform ($CDCl_3$) with TMS as the internal reference unless otherwise stated, and chemical shifts (δ) are reported in parts per million. Thermogravimetric analysis (TGA) was recorded on a PerkinElmer Pyris under a nitrogen atmosphere at a heating rate of 10 °C min^{-1}. Differential scanning calorimetry (DSC) was measured on a TA Q200 Instrument under a nitrogen atmosphere at a heating rate of 10 °C min^{-1}. Absorption spectra were obtained on an HP8453 UV-vis spectrophotometer. Electrochemical cyclic voltammetry was conducted on a CH instruments electrochemical analyzer. A carbon glass was used as the working electrode, Pt wire was used as the counter electrode, and Ag/Ag$^+$ electrode (0.01 M $AgNO_3$, 0.1 M TBAP in acetonitrile) was used as the reference electrode in a solution of dichloromethane with 0.1 M $TBAPF_6$ (tetrabutylammonium hexafluorophosphate) at 80 mV s^{-1}. CV curves were calibrated using ferrocence as the standard, and the $E_{1/2}$ of ferrocence was 0.09 V, which was calculated as the average of the two peak maxima E_{pa} and E_{pc}. The HOMO energy levels were obtained from the equation HOMO = $-(E_{ox}^{onset} - E_{1/2(ferrocene)} + 4.8)$ eV and the LUMO energy levels were obtained from the equation LUMO = $-(E_{red}^{onset} - E_{1/2(ferrocene)} + 4.8)$ eV. Polymerization was conducted in a CEM Discover System microwave reactor. Polymer average molecular weights were determined by high temperature gel permeation chromato-

Published on 13 March 2017. Downloaded by Synchrotron Radiation Library on 12/12/2017 06:44:24.

graphy (HT-GPC) with an Agilent PL-GPC 220 system using 1,2,4-trichlorobenzene (1,2,4-TCB) as the eluent below 160 °C and calibrated with polystyrene standards.

Synthesis of (*E*)-1,2-bis(2-bromothiophen-3-yl)ethene (2). To a three-neck round-bottom flask, anhydrous THF (100 mL) was introduced. $TiCl_4$ (6.9 mL, 62.2 mmol) was slowly added and the mixture was stirred at 0 °C for 15 min. Zinc powder (8.13 g, 124.3 mmol) was then added portion-wise, and the reaction mixture was refluxed for 1 h. After cooling to 0 °C, compound **1** (9.7 g, 41.5 mmol) was added. Subsequently the mixture was stirred at 40 °C for 6 h, and the solution was quenched by water (30 mL) and filtered through Celite®535. The filtrate was collected and extracted with ethyl acetate (EA) (150 mL × 3). The combined organic layer was washed with brine solution (100 mL) and dried over anhydrous $MgSO_4$. After filtration, the solvent was removed under vacuum and the residue was purified by column chromatography on silica gel (hexane/EA = 20/1). After recrystallization from EA, a yellow solid **2** (yield: 84%) was obtained. ^{1}H NMR ($CDCl_3$, 400 MHz): δ 7.27 (d, J = 5.6 Hz, 2 H), 7.25 (d, J = 6.0 Hz, 2 H), 6.97 (s, 2 H); ^{13}C NMR ($CDCl_3$, 100 MHz): δ 137.94, 126.18, 124.63, 122.72, 111.73; MS (HREI, $C_{10}H_6S_2Br_2$): calcd, 347.8272; found, 347.8283.

Synthesis of (*E*)-1,2-bis(2-(4-octyltetradec-1-yn-1-yl)thiophen-3-yl)ethene (3). To a deoxygenated solution of compound **2** (1000 mg, 2.87 mmol) in THF (15 mL) and diisopropylamine (15 mL), $Pd(PPh_3)_2Cl_2$ (500 mg, 0.71 mmol, 25 mol%), CuI (140 mg, 0.71 mmol, 25 mol%), PPh_3 (190 mg, 0.71 mmol, 25 mol%) and 9-(prop-2-yn-1-yl)nonadecane (2.2 g, 7.19 mmol) were added. After the mixture was stirred for 12 h at 80 °C, water (15 mL) and hydrochloric acid (2 M, 15 mL) were added. The resulting mixture was extracted with EA (30 mL × 3), and the combined organic layer was dried over anhydrous $MgSO_4$, filtered, and concentrated *in vacuo*. The residue was purified by column chromatography on silica gel (hexane/EA = 20/1) to give a yellow oil **3** (yield: 78%). ^{1}H NMR ($CDCl_3$, 400 MHz): δ 7.25 (d, J = 5.2 Hz, 2 H), 7.19 (s, 2 H), 7.10 (d, J = 5.2 Hz, 2 H), 2.52 (d, J = 5.6 Hz, 4 H), 1.67–1.64 (m, 2 H), 1.46–1.27 (m, 64 H), 0.91–0.87 (m, 12 H); ^{13}C NMR ($CDCl_3$, 100 MHz): δ 142.19, 125.11, 123.78, 122.60, 121.36, 97.96, 73.98, 37.30, 33.73, 31.94, 31.93, 30.00, 29.72, 29.67, 29.38, 26.92, 26.84, 24.25, 22.71, 14.13; MS (HREI, $C_{54}H_{88}S_2$): calcd, 800.6322; found, 800.6327.

Synthesis of 4,9-bis(2-octyldodecyl)naphtho[2,1-*b*:6,5-*b*′]dithiophene (4,9-β-aNDT). To a deoxygenated *N*-methyl-2-pyrrolidone (NMP, 2.5 mL) solution of compound **3** (500 mg, 0.96 mmol), 1,8-diazabicycloundec-7-ene (DBU) was added (0.16 mL, 1.1 mmol). After the mixture was refluxed for 2 days, the solution was cooled to room temperature, diluted with water (20 mL) and extracted with EA (10 mL × 3). The combined organic layer was washed with brine solution (5 mL) and dried over anhydrous $MgSO_4$. After filtration, the solvent was removed under vacuum and the residue was purified by column chromatography on silica gel (hexane) to give a green solid **4,9-β-aNDT** (yield: 88%). ^{1}H NMR ($CDCl_3$, 400 MHz): δ 8.24 (d, J = 5.6 Hz, 2 H), 7.90 (s, 2 H), 7.54 (d, J = 5.6 Hz, 2 H), 3.42 (d, J = 7.2 Hz, 4 H), 2.17–2.13 (m, 2H), 1.39–1.28 (m, 64H), 0.99–0.94 (m, 12 H); ^{13}C NMR ($CDCl_3$, 100 MHz): δ 138.37, 134.65, 133.97, 128.76, 126.79, 123.98, 123.06, 43.69, 36.49, 33.14, 32.04, 32.00, 30.15, 29.75, 29.72, 29.66, 29.47, 29.41, 26.11, 22.80, 22.78, 14.19; MS (HREI, $C_{54}H_{88}S_2$): calcd, 800.6322; found, 800.6323.

Synthesis of 2,7-dibromo-4,9-bis(2-octyldodecyl)naphtho[2,1-*b*:6,5-*b*′]dithiophene (Br-4,9-β-aNDT). To a solution of **4,9-β-aNDT** (1.1 g, 1.37 mmol) in $CHCl_3$ (120 mL) combined with acetic acid (20 mL), *N*-bromosuccinimide (0.5 g, 2.75 mmol) was added at room temperature. After the reaction mixture was stirred for 12 h at room temperature in the dark, the solution was quenched by water (30 mL) and extracted with EA (100 mL × 3). The collected organic layer was dried over $MgSO_4$. After removal of the solvent under vacuum, the residue was purified by column chromatography on silica gel (hexane) and then recrystallized from hexane to give a white solid **Br-4,9-β-aNDT** (yield: 73%) ^{1}H NMR ($CDCl_3$, 400 MHz): δ 8.14 (s, 2 H), 7.66 (s, 2 H), 7.54(d, J = 5.6 Hz, 2 H), 3.26 (d, J = 7.2 Hz, 4 H), 1.96–1.92 (m, 2H), 1.29–1.03 (m, 64 H), 0.90–0.85 (m, 12 H); ^{13}C NMR ($CDCl_3$, 100 MHz): δ 139.50, 138.55, 138.47, 134.28, 131.73, 127.97, 124.36, 36.96, 32.77, 32.73, 31.92, 31.90, 30.23, 29.73, 29.67, 29.64, 29.35, 29.32, 26.14, 26.12, 22.68, 22.66, 14.11; MS (HRFD, $C_{54}H_{86}S_2Br_2$): calcd, 956.4532; found, 956.4546.

Synthesis of 5-octyl-1-(thiophen-3-yl)pentadec-2-yn-1-one (5). To a solution of 9-(prop-2-yn-1-yl)nonadecane (3 g, 9.8 mmol) in anhydrous THF (35 ml) at 0 °C, *n*-BuLi (2.5 M, 3.7 mL, 9.4 mmol) was added dropwise. After stirring for 30 min, compound **4** (1 g, 8.92 mmol) was added and the solution was slowly warmed to room temperature. The crude residue was concentrated under vacuum. After the addition of CH_2Cl_2 (80 mL) and pyridinium chlorochromate (PCC) (2.4 g, 11.15 mmol), the solution was stirred for 30 min at room temperature. The mixture was quenched by water (15 mL) and filtered through Celite®535. The filtrate was collected and extracted with EA (60 mL × 3). The combined organic layer was washed with brine solution (40 mL) and dried over anhydrous $MgSO_4$. After filtration, the solvent was removed under vacuum and the residue was purified by column chromatography on silica gel (hexane/EA = 20/1) to obtain a yellow oil **5** (yield: 83%). ^{1}H NMR ($CDCl_3$, 400 MHz): δ 8.23–8.22 (m, 1 H), 7.61–7.59 (m, 1 H), 7.32–7.30 (m, 1 H), 2.46 (d, J = 5.6 Hz, 2 H), 1.68–1.64 (m, 1 H), 1.43–1.26 (m, 32 H), 0.89–0.83 (m, 6 H); ^{13}C NMR ($CDCl_3$, 100 MHz): δ 171.63, 143.26, 134.98, 126.80, 126.53, 94.04, 81.14, 36.90, 33.73, 31.89, 31.87, 29.83, 29.64, 29.62, 29.57, 29.32, 29.30, 26.77, 23.43, 22.66, 14.09; MS (HREI, $C_{27}H_{44}OS$): calcd, 416.3107; found, 416.3098.

Synthesis of (*E*)-3,3′-(11,20-dioctyltriaconta-15-en-13,17-diyne-15,16-diyl)dithiophene (6). To a three-neck round-bottom flask containing compound **5** (6 g, 14.4 mmol) and anhydrous THF (200 mL), $TiCl_4$ (2.4 mL, 21.6 mmol) was slowly added. The mixture was stirred at 0 °C for 15 min. Zinc powder (2.8 g, 43.2 mmol) was then added portion-wise. After the solution was stirred at room temperature for 3 h, the mixture was quenched by water (30 mL) and filtered through Celite®535. The filtrate was collected and extracted with EA (120 mL × 3). The combined organic layer was washed with

 This journal is © The Royal Society of Chemistry 2017

Published on 13 March 2017. Downloaded by Synchrotron Radiation Library on 12/12/2017 06:44:24.

brine solution (200 mL) and dried over anhydrous $MgSO_4$. After filtration, the solvent was removed under vacuum and the residue was purified by column chromatography on silica gel (hexane/EA = 20/1) to obtain a yellow oil **6** (yield: 79%). ^{1}H NMR ($CDCl_3$, 400 MHz): δ 7.89–7.88 (m, 2 H), 7.72–7.71 (m, 2 H), 7.24–7.22 (m, 2 H), 2.43(d, J = 5.6 Hz, 4 H), 1.92–1.90 (m, 1 H), 1.51–1.28 (m, 64 H), 0.91–0.88 (m, 6 H); ^{13}C NMR ($CDCl_3$, 100 MHz): δ 140.49, 128.79, 124.97, 123.51, 120.69, 98.86, 82.73, 37.30, 36.84, 33.75, 33.34, 31.91, 29.95, 29.89, 29.69, 29.68, 29.64, 29.60, 29.35, 29.32, 26.87, 26.75, 26.69, 24.26, 22.68, 22.62, 14.10; MS (HREI, $C_{54}H_{88}S_2$): calcd, 800.6322; found, 800.6335.

Synthesis of 5,10-bis(2-octyldodecyl)naphtho[2,1-*b*:6,5-*b*′] dithiophene (5,10-β-aNDT). In a similar manner to the preparation of **4,9-β-aNDT**, **5,10-β-aNDT** was synthesized from compound **6**. ^{1}H NMR ($CDCl_3$, 400 MHz): δ 8.05 (d, J = 5.6 Hz, 2 H), 8.00 (s, 2 H), 7.59 (d, J = 5.6 Hz, 2 H), 2.98 (d, J = 7.2 Hz, 4 H), 2.10–2.07 (m, 1 H), 1.43–1.23 (m, 64 H), 0.89–0.84 (m, 6 H); ^{13}C NMR ($CDCl_3$, 100 MHz): δ 138.16, 136.27, 133.61, 125.92, 125.19, 122.67, 120.28, 40.64, 37.51, 36.85, 33.69, 33.35, 31.92, 31.89, 30.02, 29.90, 29.71, 29.67, 29.64, 29.61, 29.34, 29.33, 26.76, 26.55, 22.69, 22.66, 22.6, 14.11; MS (HREI, $C_{54}H_{88}S_2$): calcd, 800.6322; found, 800.6333.

Synthesis of 2,7-dibromo-5,10-bis(2-octyldodecyl)naphtho [2,1-*b*:6,5-*b*′]dithiophene (Br-5,10-β-aNDT). In a similar manner to the preparation of **Br-4,9-β-aNDT**, **Br-5,10-β-aNDT** was synthesized from **5,10-β-aNDT**. ^{1}H NMR ($CDCl_3$, 400 MHz): δ 8.15 (s, 2 H), 7.68 (s, 2 H), 3.49 (d, J = 5.6 Hz, 4 H), 1.98–1.93 (m, 1 H), 1.41–1.04 (m, 64 H), 0.97–0.85 (m, 6 H); ^{13}C NMR ($CDCl_3$, 100 MHz): δ 137.59, 135.91, 134.25, 128.17, 125.85, 123.71, 123.60, 36.84, 33.35, 31.92, 29.91, 29.67, 29.66, 29.61, 29.37, 29.34, 26.76, 22.68, 22.59, 14.05; MS (HRFD, $C_{54}H_{86}S_2Br_2$): calcd, 956.4532; found, 956.4545.

Synthesis of P4,9-βNDTDTFBT. Br-4,9-β-aNDT (210 mg, 0.219 mmol), 4,7-bis(5-(trimethylstannyl)thiophen-2-yl)-5,6-difluorobenzo[*c*][1,2,5]thiadiazole (145 mg, 0.219 mmol), $Pd_2(dba)_3$ (8 mg, 0.009 mmol), tri(*o*-tolyl)phosphine (21 mg, 0.070 mmol) and dry chlorobenzene (5 mL) were introduced to a 50 mL round-bottom flask. The mixture was deoxygenated with nitrogen for 30 min at room temperature. The reaction was then carried out in a microwave reactor under 270 W for 50 min. In order to end-cap the resultant polymer, tributyl (thiophen-2-yl)stannane (41 mg, 0.108 mmol) was added to the mixture, and the microwave reaction was continued for 10 min under 270 W. Subsequent to the addition of tributyl (thiophen-2-yl)stannane, another end-capping reagent, 2-bromothiophene (19.4 mg, 0.119 mmol) was added and the reaction was continued for another 10 min under otherwise identical conditions. The mixture was then added into methanol dropwise. The precipitate was collected by filtration and washed by Soxhlet extraction with acetone, hexane, THF, chloroform, toluene and chlorobenzene sequentially for 5 days. The crude polymer was dissolved in hot chlorobenzene and the residual Pd catalyst and Sn metal in the chlorobenzene solution were removed by Pd–thiol gel and Pd–TAAcOH (Silicycle Inc.). After filtration and removal of the solvent, the polymer was redissolved in chlorobenzene and reprecipitated by methanol. The resultant polymer was collected by filtration and dried under vacuum for 1 day to afford a deep-blue solid. (212 mg, 85%) ^{1}H NMR ($CDCl_3$: CS_2 = 1 : 1, 400 MHz): δ 8.40–8.05 (br, 4 H), 7.94–7.82 (br, 2 H), 7.52–7.41 (br, 2 H), 3.61–3.22 (br, 4 H), 2.03–1.97 (br, 2 H), 1.80–0.80 (br, 104 H).

Synthesis of P5,10—βNDTDTFBT. Br-5,10-β-aNDT (273 mg, 0.285 mmol), 4,7-bis(5-(trimethylstannyl)thiophen-2-yl)-5,6-difluorobenzo[*c*][1,2,5]thiadiazole (189 mg, 0.285 mmol), $Pd_2(dba)_3$ (10 mg, 0.012 mmol), tri(*o*-tolyl)phosphine (27 mg, 0.091 mmol), and dry chlorobenzene (7 mL) were introduced to a 50 mL round-bottom flask. The mixture was deoxygenated with nitrogen for 30 min at room temperature. The reaction was then carried out in a microwave reactor under 270 W for 50 min. In order to end-cap the resultant polymer, tributyl (thiophen-2-yl)stannane (53 mg, 0.140 mmol) was added to the mixture, and the microwave reaction was continued for 10 min under 270 W. Subsequent to the addition of tributyl (thiophen-2-yl)stannane, another end-capping reagent, 2-bromothiophene (25 mg, 0.155 mmol) was added and the reaction was continued for another 10 min under otherwise identical conditions. The mixture was then added into methanol dropwise. The precipitate was collected by filtration and washed by Soxhlet extraction with acetone, hexane, THF, chloroform, toluene and chlorobenzene sequentially for 6 days. The crude polymer was dissolved in hot chlorobenzene and the residual Pd catalyst and Sn metal in the chlorobenzene solution were removed by Pd–thiol gel and Pd–TAAcOH (Silicycle Inc.). After filtration and removal of the solvent, the polymer was redissolved in chlorobenzene and reprecipitated by methanol. The resultant polymer was collected by filtration and dried under vacuum for 1 day to afford a deep-blue solid. (298 mg, 92%) ^{1}H NMR ($CDCl_3$: CS_2 = 1 : 1, 400 MHz): δ 8.41–8.03 (br, 4 H), 7.94–7.82 (br, 2 H), 7.52–7.41 (br, 2 H), 3.63–3.41 (br, 4 H), 2.19–2.17 (br, 2 H), 1.80–0.70 (br, 104 H).

Fabrication and characterization of OFET devices

300 nm thick SiO_2 was deposited on n-doped silicon wafers (Ci = 11 nF cm^{-2}). The substrates were rinsed with sulfuric acid and hydrogen peroxide (30% solution in water) (3 : 1, volume ratio) at room temperature for 1 h, followed by 15 min of sonication in pure water. The substrates were heated on a hot plate in a glovebox at 150 °C to remove water, followed by UV-ozone treatment for 30 min. The SiO_2 wafers were immersed in an octadecyltrichlorosilane (ODTS) : toluene solution (1 : 100, volume ratio) for 3 h. The surface of the ODTS-treated SiO_2/Si substrates was washed with acetone and heated for 1 h at 100 °C. Thin films (40–60 nm in thickness) of the polymers were deposited on ODTS-treated SiO_2/Si substrates by spin-coating (1000 rpm) their hot $CHCl_3$ solutions (10 mg mL^{-1}). Thermal annealing was then conducted at 200 °C for 10 min. A gold source and drain contacts (40 nm in thickness) were deposited by vacuum evaporation on the polymer layer to complete the bottom-gate/top-contact OFET devices. Electrical measurements of all OFET devices were carried out at room temperature in air on a 4156C instrument (Agilent

Published on 13 March 2017. Downloaded by Synchrotron Radiation Library on 12/12/2017 06:44:24.

Technologies). The field-effect mobility was calculated at saturation using the equation $I_{ds} = (\mu WC_i/2L)(V_g - V_t)^2$, where I_{ds} is the drain–source current, μ is the field-effect mobility, W is the channel width (1 mm), L is the channel length (100 μm), C_i is the capacitance per unit area of the gate dielectric layer, V_g is the gate voltage, and V_t is the threshold voltage.

Fabrication and characterization of OPV devices

For the inverted architectures, a ZnO precursor solution was spin coated onto ITO-coated glass and followed by thermal annealing at 170 °C in air for 15 min to crystallize the film (thickness = *ca.* 50 nm). The detailed processing parameters (polymer/ODCB concentration; spin coating speed) are as follows: **P4,9-βNDTDTFBT**/$PC_{71}BM$ (15 mg mL^{-1}; 1200 rpm) and **P5,10-βNDTDTFBT**/$PC_{71}BM$ (15 mg mL^{-1}; 1200 rpm). An MoO_3 layer (thickness = *ca.* 7 nm) and silver top anode (thickness = *ca.* 150 nm) were then thermally evaporated through a shadow mask under high vacuum (<1×10^{-6} Torr) to complete the inverted devices. Each device was constituted of 4 pixels defined by an active area of 0.04 cm^2. Finally, the *J–V* curves were measured in air under an AM 1.5 G spectrum from a solar simulator.

Acknowledgements

We thank the Ministry of Science and Technology, the Ministry of Education, and the Center for Interdisciplinary Science (CIS) of the National Chiao Tung University, Taiwan, for financial support. We thank the National Center of High-Performance Computing (NCHC) in Taiwan for computer time and facilities. Y. J. C. acknowledges the support from the Golden-Jade fellowship of the Kenda Foundation, Taiwan. H. Y. thanks Hong Kong Innovation and Technology Commission for the support through ITC-CNERC14SC01.

References

1 G. Yu, J. Gao, J. C. Hummelen, F. Wudl and A. J. Heeger, *Science*, 1995, **270**, 1789–1791.
2 M. C. Scharber, D. Mühlbacher, M. Koppe, P. Denk, C. Waldauf, A. J. Heeger and C. J. Brabec, *Adv. Mater.*, 2006, **18**, 789–794.
3 Y.-J. Cheng, S.-H. Yang and C.-S. Hsu, *Chem. Rev.*, 2009, **109**, 5868–5923.
4 X. Zhao and X. Zhan, *Chem. Soc. Rev.*, 2011, **40**, 3728–3743.
5 J.-S. Wu, S.-W. Cheng, Y.-J. Cheng and C.-S. Hsu, *Chem. Soc. Rev.*, 2015, **44**, 1113–1154.
6 B. Fan, C. Sun, X.-F. Jiang, G. Zhang, Z. Chen, L. Ying, F. Huang and Y. Cao, *Adv. Funct. Mater.*, 2016, **26**, 6479–6488.
7 X. Guo, M. Zhang, W. Ma, L. Ye, S. Zhang, S. Liu, H. Ade, F. Huang and J. H. Hou, *Adv. Mater.*, 2014, **26**, 4043–4049.
8 L. Ye, S. Q. Zhang, W. Ma, B. H. Fan, X. Guo, Y. Huang, H. Ade and J. H. Hou, *Adv. Mater.*, 2012, **24**, 6335–6341.
9 Q. Zheng, B. J. Jung, J. Sun and H. E. Katz, *J. Am. Chem. Soc.*, 2010, **132**, 5394–5404.
10 M. Wang, D. Cai, Z. Yin, S.-C. Chen, C.-F. Du and Q. Zheng, *Adv. Mater.*, 2016, **28**, 3359–3365.
11 T. Wang, H. Wang, G. Li, M. Li, Z. Bo and Y. Chen, *Macromolecules*, 2016, **49**, 4088–4094.
12 H. Lu, J. Zhang, J. Chen, Q. Liu, X. Gong, S. Feng, X. Xu, W. Ma and Z. Bo, *Adv. Mater.*, 2016, **28**, 9559–9566.
13 J. Zhang, X. Zhang, G. Li, H. Xiao, W. Li, S. Xie, C. Li and Z. Bo, *Chem. Commun.*, 2016, **52**, 469–472.
14 K. Zhang, K. Gao, R. Xia, Z. Wu, C. Sun, J. Cao, L. Qian, W. Li, S. Liu, F. Huang, X. Peng, L. Ding, H. L. Yip and Y. Cao, *Adv. Mater.*, 2016, **28**, 4817–4823.
15 Z. Qi, J. Cao, H. Li, L. Ding and J. Wang, *Adv. Funct. Mater.*, 2015, **25**, 3138–3146.
16 H. Kang, M. A. Uddin, C. Lee, K.-H. Kim, T. L. Nguyen, W. Lee, Y. Li, C. Wang, H. Y. Woo and B. J. Kim, *J. Am. Chem. Soc.*, 2015, **137**, 2359–2365.
17 S. Y. Son, Y. Kim, J. Lee, G.-Y. Lee, W.-T. Park, Y.-Y. Noh, C. E. Park and T. Park, *J. Am. Chem. Soc.*, 2016, **138**, 8096–8103.
18 S. Xiao, Q. Zhang and W. You, *Adv. Mater.*, 2016, 1601391.
19 L. Lu, M. A. Kelly, W. You and L. Yu, *Nat. Photonics*, 2015, **9**, 491–500.
20 Z. Zhao, F. J. Zhang, X. Zhang, X. D. Yang, H. X. Li, X. K. Gao, C.-A. Di and D. B. Zhu, *Macromolecules*, 2013, **46**, 7705–7714.
21 X. Guo, A. Facchetti and T. J. Marks, *Chem. Rev.*, 2014, **114**, 8943–9021.
22 J. Chen and Y. Cao, *Acc. Chem. Res.*, 2009, **42**, 1709–1718.
23 N. Blouin, A. Michaud, D. Gendron, S. Wakim, E. Blair, R. Neagu-Plesu, M. Belletete, G. Durocher, Y. Tao and M. Leclerc, *J. Am. Chem. Soc.*, 2008, **130**, 732–742.
24 V. Vohra, K. Kawashima, T. Kakara, T. Koganezawa, I. Osaka, K. Takimiya and H. Murata, *Nat. Photonics*, 2015, **9**, 403–408.
25 K. Kawashima, T. Fukuhara, Y. Suda, Y. Suzuki, T. Koganezawa, H. Yoshida, H. Ohkita, I. Osaka and K. Takimiya, *J. Am. Chem. Soc.*, 2016, **138**, 10265–10275.
26 I. McCulloch, R. S. Ashraf, L. Biniek, H. Bronstein, C. Combe, J. E. Donaghey, D. I. James, C. B. Nielsen, B. C. Schroeder and W. Zhang, *Acc. Chem. Res.*, 2012, **45**, 714–722.
27 J.-W. Jung, F. Liu, T. P. Russell and W.-H. Jo, *Energy Environ. Sci.*, 2013, **6**, 3301–3307.
28 Y.-H. Chao, J.-F. Jheng, J.-S. Wu, K.-Y. Wu, H.-H. Peng, M.-C. Tsai, C.-L. Wang, Y.-N. Hsiao, C.-L. Wang, C.-Y. Lin and C.-S. Hsu, *Adv. Mater.*, 2014, **26**, 5205–5210.
29 D. L. Liu, W. C. Zhao, S. Q. Zhang, L. Ye, Z. Zheng, Y. Cui, Y. Chen and J. H. Hou, *Macromolecules*, 2015, **48**, 5172–5178.
30 J. D. Chen, C. Cui, Y. Q. Li, L. Zhou, Q. D. Ou, C. Li, Y. Li and J. X. Tang, *Adv. Mater.*, 2015, **27**, 1035–1041.
31 H. F. Yao, L. Ye, H. Zhang, S. S. Li, S. Q. Zhang and J. H. Hou, *Chem. Rev.*, 2016, 7397.

 This journal is © The Royal Society of Chemistry 2017

Published on 13 March 2017. Downloaded by Synchrotron Radiation Library on 12/12/2017 06:44:24.

32 J. Y. Wang, K. L. Shi, Y. Suo, Y. Z. Lin, G. Yu and X. W. Zhan, *J. Mater. Chem. C*, 2016, **4**, 3781–3791.
33 W. Li, B. Guo, C. Chang, X. Guo, M. Zhang and Y. Li, *J. Mater. Chem. A*, 2016, **4**, 10135–10141.
34 H. Bin, Z.-G. Zhang, L. Gao, S. Chen, L. Zhong, L. Xue, C. Yang and Y. Li, *J. Am. Chem. Soc.*, 2016, **138**, 4657–4664.
35 Q. Zhang, M. A. Kelly, A. Hunt, H. Ade and W. You, *Macromolecules*, 2016, **49**, 2533–2540.
36 T. Okamoto, Y. Jiang, F. Qu, A. C. Mayer, J. E. Parmer, M. D. McGehee and Z. Bao, *Macromolecules*, 2008, **41**, 6977–6980.
37 Y. Jiang, T. Okamoto, H. A. Becerril, S. Hong, M. L. Tang, A. C. Mayer, J. E. Parmer, M. D. McGehee and Z. Bao, *Macromolecules*, 2010, **43**, 6361–6367.
38 J.-S. Wu, C.-T. Lin, C.-L. Wang, Y.-J. Cheng and C.-S. Hsu, *Chem. Mater.*, 2012, **24**, 2391–2399.
39 M. Nakano, K. Niimi, E. Miyazaki, I. Osaka and K. Takimiya, *J. Org. Chem.*, 2012, **77**, 8099–8111.
40 H. T. Yi, M. M. Payne, J. E. Anthony and V. Podzorov, *Nat. Commun.*, 2012, **3**, 1259.
41 I. Nasrallah, K. K. Banger, Y. Vaynzof, M. M. Payne, P. Too, J. Jongman, J. E. Anthony and H. Sirringhaus, *Chem. Mater.*, 2014, **26**, 3914–3919.
42 L. Yu, X. Li, E. Pavlica, F. P. V. Koch, G. Portale, I. da Silva, M. A. Loth, J. E. Anthony, P. Smith, G. Bratina, B. K. C. Kjellander, C. W. M. Bastiaansen and D. J. Broer, *Chem. Mater.*, 2013, **25**, 1823–1828.
43 M. M. Payne, S. R. Parkin, J. E. Anthony, C.-C. Kuo and T. N. Jackson, *J. Am. Chem. Soc.*, 2005, **127**, 4986–4987.
44 W. H. Lee, D. Kwak, J. E. Anthony, H. S. Lee, H. H. Choi, D. H. Kim, S. G. Lee and K. Cho, *Adv. Funct. Mater.*, 2012, **22**, 267–281.
45 O. D. Jurchescu, S. Subramanian, R. J. Kline, S. D. Hudson, J. E. Anthony, T. N. Jackson and D. J. Gundlach, *Chem. Mater.*, 2008, **20**, 6733–6737.
46 S.-W. Cheng, D.-Y. Chiou, Y.-Y. Lai, R.-H. Yu, C.-H. Lee and Y.-J. Cheng, *Org. Lett.*, 2013, **15**, 5338–5341.
47 S. Shinamura, E. Miyazaki and K. Takimiya, Synthesis, *J. Org. Chem.*, 2010, **75**, 1228–1234.
48 I. Osaka, S. Shinamura, T. Abe and K. Takimiya, *J. Mater. Chem. C*, 2013, **1**, 1297–1304.
49 Z. Wu, T. Yang, B. S. Ong, Y. Liang and X. Guo, *Org. Photonics Photovolt.*, 2014, **2**, 21–39.
50 S.-W. Cheng, C.-E. Tsai, W.-W. Liang, Y.-L. Chen, F.-Y. Cao, C.-S. Hsu and Y.-J. Cheng, *Macromolecules*, 2015, **48**, 2030–2038.
51 S.-W. Cheng, D.-Y. Chiou, C.-E. Tsai, W.-W. Liang, C.-Y. Hsu, Y.-Y. Lai, C.-S. Hsu, I. Osaka, K. Takimiya and Y.-J. Cheng, *Adv. Funct. Mater.*, 2015, **25**, 6131–6143.
52 S. Shinamura, I. Osaka, E. Miyazaki, A. Nakao, M. Yamagishi, J. Takeya and K. Takimiya, *J. Am. Chem. Soc.*, 2011, **133**, 5024–5035.
53 I. Osaka, T. Abe, S. Shinamura and K. Takimiya, *J. Am. Chem. Soc.*, 2011, **133**, 6852–6860.
54 S. Shi, P. Jiang, S. Yu, L. Wang, X. Wang, M. Wang, H. Wang, Y. Li and X. Li, *J. Mater. Chem. A*, 2013, **1**, 1540–1543.
55 M. Mamada, T. Minamiki, H. Katagiri and S. Tokito, *Org. Lett.*, 2012, **14**, 4062–4065.
56 D. Lehnherr, A. R. Waterloo, K. P. Goetz, M. M. Payne, F. Hampel, J. E. Anthony, O. D. Jurchescu and R. R. Tykwinski, *Org. Lett.*, 2012, **14**, 3660–3663.
57 K. R. Graham, C. Cabanetos, J. P. Jahnke, M. N. Idso, A. El Labban, G. O. Ngongang Ndjawa, T. Heumueller, K. Vandewal, A. Salleo, B. F. Chmelka, A. Amassian, P. M. Beaujuge and M. D. McGehee, *J. Am. Chem. Soc.*, 2014, **136**, 9608–9618.
58 C. Lee, H. Kang, W. Lee, T. Kim, K.-H. Kim, H. Y. Woo, C. Wang and B. J. Kim, *Adv. Mater.*, 2015, **27**, 2466–2471.
59 I. Osaka, Y. Houchin, M. Yamashita, T. Kakara, N. Takemura, T. Koganezawa and K. Takimiya, *Macromolecules*, 2014, **47**, 3502–3510.
60 I. Meager, R. S. Ashraf, S. Mollinger, B. C. Schroeder, H. Bronstein, D. Beatrup, M. S. Vezie, T. Kirchartz, A. Salleo, J. Nelson and I. McCulloch, *J. Am. Chem. Soc.*, 2013, **135**, 11537–11540.
61 G. Ren, P.-T. Wu and S. A. Jenekhe, *Chem. Mater.*, 2010, **22**, 2020–2026.
62 S. Ko, E. T. Hoke, L. Pandey, S. Hong, R. Mondal, C. Risko, Y. Yi, R. Noriega, M. D. McGehee, J.-L. Brédas, A. Salleo and Z. Bao, *J. Am. Chem. Soc.*, 2012, **134**, 5222–5232.
63 B. Burkhart, P. P. Khlyabich and B. C. Thompson, *Macromolecules*, 2012, **45**, 3740–3748.
64 C.-H. Cho, H. J. Kim, H. Kang, T. J. Shin and B. J. Kim, *J. Mater. Chem.*, 2012, **22**, 14236–14245.
65 Y. Liu, J. Zhao, Z. Li, C. Mu, W. Ma, H. Hu, K. Jiang, H. Lin, H. Ade and H. Yan, *Nat. Commun.*, 2014, **5**, 5293.